Effects of Hill Shapes
on Tsunami Simulations

Kristian Pedersen and Gustav Baardsen

October 15, 2012

Abstract

In this project we study how the shape of hills at the sea bottom affects numerical and physical properties of simulations of earthquake-generated tsunamis. The tsunamis are modelled using two-dimensional wave equations, and a finite difference scheme is used to solve the partial differential equations.

Contents

1 Introduction

In this text we will address a two-dimensional, standard linear wave equation, with damping and reflecting boundaries. We will develop a scheme for solving it and apply it to the problem of a tsunami over an uneven seabed. Especial focus will be put on the question of which kinds of seabeds causes numerical instability.

2 Mathematical model

For (x, y) in the domain $D = [0, L_y] \times [0, L_x]$ and $t \in [0, T]$, we will study the partial differential equation

$$u_{tt} + bu_t = (q(x, y)u_x)_x + (q(x, y)u_y)_y + f(x, y, t), \tag{1}$$

where $(x, y) \in D$ and $t \in [0, T]$, with the boundary and initial conditions

$$\frac{\partial u}{\partial n} = 0 \qquad\qquad (x, y) \in \partial D, t \in [0, T],$$
$$u(x, y, 0) = I(x, y) \qquad\qquad x, y \in \partial D,$$
$$u_t(x, y, 0) = V(x, y) \qquad\qquad x, y \in \partial D. \tag{2}$$

Here ∂D denotes the boundary of the domain D and $\partial/\partial n$ stands for differentiation in the normal direction out of the boundary.

3 Numerical scheme

3.1 Numerical scheme for the inner points

In operator notation, we want to use the following scheme for inner points:

$$[D_t D_t u + b D_{2t} u = D_x(q D_x u) + D_y(q D_y u) + f]_{i\,j}^n \tag{3}$$

Calculating each summand we find:

$$[D_t D_t u]_{i\,j}^n = \frac{u_{i,j}^{n+1} - 2u_{i,j}^n + u_{i,j}^{n-1}}{\Delta t^2}, \tag{4}$$

$$[b D_2 t u]_{i\,j}^n = b\frac{u_{i,j}^{n+1} - u_{i,j}^{n-1}}{2\Delta t}, \tag{5}$$

$$[D_x q D_x u]_{i\,j}^n = \frac{q_{i+\frac{1}{2},j}(u_{i+1,j}^n - u_{i,j}^n) - q_{i-\frac{1}{2},j}(u_{i,j}^n - u_{i-1,j}^n)}{\Delta x^2}, \tag{6}$$

$$[D_y q D_y u]_{i\,j}^n = \frac{q_{i,j+\frac{1}{2}}(u_{i,j+1}^n - u_{i,j}^n) - q_{i,j-\frac{1}{2}}(u_{i,j}^n - u_{i,j-1}^n)}{\Delta x^2}, \tag{7}$$

$$[f]_{i\,j}^n = f(x_i, y_j, t_n). \tag{8}$$

Inserting these expressions into Eq. (3) and solving for $u_{i,j}^{n+1}$, we get the following scheme for inner points:

$$u_{i,j}^{n+1} = \{2u_{i,j}^n + u_{i,j}^{n-1}$$
$$+\frac{\Delta t^2}{\Delta x^2}\left(q_{i+\frac{1}{2},j}(u_{i+1,j}^n - u_{i,j}^n) - q_{i-\frac{1}{2},j}(u_{i,j}^n - u_{i-1,j}^n)\right)$$
$$+\frac{\Delta t^2}{\Delta y^2}\left(q_{i,j+\frac{1}{2}}(u_{i,j+1}^n - u_{i,j}^n) - q_{i,j-\frac{1}{2}}(u_{i,j}^n - u_{i,j-1}^n)\right)$$
$$+\Delta t^2 f(x_i, y_j, t_n)\} / \left(1 + \frac{1}{2}b\Delta t\right) \tag{9}$$

3.2 Numerical scheme for the first time step

For the first time step $n = 0$, $u_{i,j}^{n-1}$ is not a part of the grid. To circumvent this problem, we have to apply the intial condition $u_t(x, y, 0) = V(x, y)$ for $x, y \in \partial D$. We discretize it and get:

$$[D_{2t}u = V]_{ij}^0 \implies \frac{u_{ij}^1 - u_{ij}^{-1}}{2\Delta t} = V(x_i, y_j) \implies u_{ij}^{-1} = u_{ij}^1 - 2\Delta t V(x_i, y_j).$$

Inserting this into equation (4) and (5), we get:

$$[D_t D_t u]_{ij}^n = 2\left(\frac{u_{i,j}^{n+1} - u_{i,j}^n}{\Delta t^2} - \frac{V(x_i, y_i)}{\Delta t}\right), \tag{10}$$

$$[bD_{2t}u]_{ij}^n = b\frac{V(x_i, y_i)}{\Delta t}. \tag{11}$$

Inserting these expressions into Eq. (3) and solving for $u_{i,j}^{n+1}$, we get the following scheme for inner points in the first time step $n = 0$:

$$
\begin{aligned}
u_{i,j}^{n+1} = u_{i,j}^n &+ \left(1 - \frac{1}{2}b\Delta t\right)\Delta t V_{i,j} \\
&+ \frac{\Delta t^2}{2\Delta x^2}\left(q_{i+\frac{1}{2},j}(u_{i+1,j}^n - u_{i,j}^n) - q_{i-\frac{1}{2},j}(u_{i,j}^n - u_{i-1,j}^n)\right) \\
&+ \frac{\Delta t^2}{2\Delta y^2}\left(q_{i,j+\frac{1}{2}}(u_{i,j+1}^n - u_{i,j}^n) - q_{i,j-\frac{1}{2}}(u_{i,j}^n - u_{i,j-1}^n)\right) \\
&+ \frac{\Delta t^2}{2}f(x_i, y_j, t_n).
\end{aligned}
\tag{12}
$$

3.3 Numerical scheme for the boundary

On the boundary, this scheme needs points outside the defined space domain. For example, we need values for $u_{-1,j}^n$, u_{i,N_y+1}^n, and $u_{0,-1}^n$. Values for these points can be obtained from the discretized versions of the Neumann condition. The Neumann conditions are in discretized form

$$[D_{2x}u]_{0j}^n = [D_{2x}u]_{N_x j}^n = 0 \quad \text{for } j = 0, 1, \ldots, N_y, \quad n = 0, 1, \ldots, N_t, \tag{13}$$

$$[D_{2y}u]_{i0}^n = [D_{2y}u]_{0,N_y}^n = 0 \quad \text{for } i = 0, 1, \ldots, N_y, \quad n = 0, 1, \ldots, N_t, \tag{14}$$

which leads to the equations

$$u_{1,j}^n = u_{-1,j}^n, \quad u_{N_x-1,j}^n = u_{Nx+1,j}^n \quad \text{for } j = 0, 1, \ldots, N_y, \quad n = 0, 1, \ldots, N_t \tag{15}$$

$$u_{i,1}^n = u_{i,-1}^n, \quad u_{i,Ny+1}^n = u_{i,Nx+1}^n \quad \text{for } i = 0, 1, \ldots, N_y, \quad n = 0, 1, \ldots, N_t. \tag{16}$$

A scheme for the borders can now be found by applying each equality to the inner point scheme for its boundary. The corners are found by applying two equalities, one for each of the adjacent border.

3.4   Approximating q(x,y) outside the grid

In our implementation, we assume that values for the function $q(x,y)$ are given only at the grid points (x_i, y_j). In the finite difference algorithm, we use mean values to evaluate the function at other points. To approximate the q function when evaluated outside the grid, we will apply the arithmetic and harmonic mean, defined respectively as

$$q_{i+\frac{1}{2},j} = \frac{q_{i,j} + q_{i+1,j}}{2} \qquad (17)$$

$$(18)$$

and

$$q_{i+\frac{1}{2},j} = 2 \left(\frac{1}{q_{i,j}} + \frac{1}{q_{i+1,j}} \right)^{-1}. \qquad (19)$$

When not states explicitly otherwise, we have used the arithmetic mean as the default option.

4   Implementation

We implemented the code in pure python. See the wave2D_du0.py for the full code.

TODO: Show the core of the program in minted enviroment

5   Numerical experiments

5.1   Verification

The implementation of the finite difference algorithm was verified with the following tests:

- In the first test the initial conditions were set to

$$u(x, y, t = 0) \equiv I(x, y) = u_0,$$
$$u_t(x, y, t = 0) \equiv V(x, y) = 0, \qquad (20)$$

  where u_0 is a constant, and we used the restriction $f(x, y, t) = 0$. The resulting PDE gives the constant solution $u(x, y, t) = u_0$.

- In the second test case, the 2-dimensional code was tested with the simple one-dimensional plug function

$$I(x, y) = \begin{cases} 0 & \text{if } |x - L/2| > a, \\ 1 & \text{else}, \end{cases}$$

4

as initial condition. In the case with $V(x,y) = 0$, $f(x,y,t) = 0$, and $q(x,y) = c^2$, where c is a constant, the solution $u(x,y,t)$ gives exactly two moving squares, as long as the Carnot number $C \equiv c\Delta t/\Delta x$ is 1. This test was repeated by interchanging x and y in the initial condition.

- As another one-dimensional test, we used the one-dimensional initial conditions

$$I(x,y) = \exp\left(a(x - L/2)^2\right),$$
$$V(x,y) = 0, \tag{21}$$

where a is a constant, togehter with the restrictions $b = 0$ and $f(x,y,t) = 0$. These conditions give the solution

$$u(x,y,t) = \frac{1}{2}\exp\left(-a(x - ct - L_x/2)^2\right)$$
$$= +\frac{1}{2}\exp\left(-a(x + ct - L_x/2)^2\right), \tag{22}$$

at the limit when the boundaries are infinitely far away. This solution does not fulfill the boundary condition $\partial u/\partial n = 0$, but it was a useful test for the first few steps of the simulation.

- As suggested in the project description, we also used the manufactured solution

$$u(x,y,t) = \exp\left(-bt\right)\cos\left(\omega t\right)\cos\left(\frac{m_x x\pi}{L_x}\right)\cos\left(\frac{m_y y\pi}{L_y}\right), \tag{23}$$

where b is the damping parameter in the studied PDE, ω is a real constant, and m_x and m_y are integers. The solution $u(x,y,t)$ is a standing wave with the desired boundary condition $\partial u/\partial n = 0$. This manufactured solution was tested both with constant q and with the choise $q(x,y) = \exp(-x-y)$. For both cases we had to determine functions $f(x,y,t)$ such that the given manufactured solution fulfills the two-dimensional wave equation. According to the project formulation, the error ε of the solution $u(x,y,t)$ should converge as

$$\varepsilon = Dh^2, \tag{24}$$

where

$$D = D_t F_t^2 + D_x F_x^2 + D_y F_y^2, \tag{25}$$

$\Delta t = F_t h$, $\Delta x = F_x h$, $\Delta y = F_y h$, and D_i and F_i, $i \in \{t,x,y\}$, are constants.

In our implementation, the convergence rate r was estimated by assuming the relation between rates of subsequent errors ε_k with decreasing parameter h_k and rates of the convergence parameter h_k being of the form

$$\frac{\varepsilon_{h_{k-1}}}{\varepsilon_{h_k}} = \left(\frac{h_{k-1}}{h_k}\right)^r. \tag{26}$$

Table 1: Convergence rates r_k for different convergence parameters h_k and two different choises of the function $q(x, y)$.

h_k	$q = $ const.	$q(x, y) = \exp(-x - y)$
0.01	1.959	1.984
0.001	1.996	1.998

Here the considered error was chosen to be

$$\varepsilon_{h_k} = \max_{i,j} \left| u_e(x_i, y_j, t_N) - u_{h_k i,j}^N \right|, \tag{27}$$

where $u_e(x, y, t)$ is the exact solution and $u_{h_k i,j}^N$ is the numerical solution with convergence parameter h_k. Examples of calculated convergence rates are given in Table 5.1.

5.2 One-dimensional simulations

We did some simulations with one-dimensional systems to get a better view of the behaviour of the solutions. With the one-dimensional systems, it was also possible to use finer mesh grids. In the directories `movie_1dwave_box_Ba250` and `movie_1dwave_gaussian_Bs250` we have examples of simulations of one-dimensional systems with a box and a Gaussian shaped hill, respectively. With the same hight of the hill, the simulation with a Gaussian perturbation gave a smoother function $u(x, y, t)$ than what was the case with the box-shaped perturbation.

Even if the solution of the Gaussian case is partially sharp, the numerical result becomes quite smooth when adding more space grid points. In the directories `movie_1dwave_gaussian_Bs275_Nx100` and
`movie_1dwave_gaussian_Bs275_Nx200`, there are simulation results obtained with the same Gaussian perturbation, whence the number of space grid points was 100 and 200 in the two runs, respectively. From these movies one clearly sees that the numerical solution becomes smooth when using a finer space mesh.

We also did a comparison between two simulations with the same box perturbation and 100 versus 200 mesh grid points. As in the case with a Gaussian hill, the numerical solution improved with a finer mesh. However, it seems that the system with a box hill may have a solution that is not smooth for any number of space mesh points. It is difficult to say, based on these simulations, what is numerical noise and what is due to a mathematically oscillating or non-smooth function. A first step in investigating that could be to compare numbers for $u_{i,\,j}^n$ of simulations with different numbers of grid points, using large N_x. It would perhaps also be instructive to look for exact numerical solutions for simple cases with a discontinuous q function.

Another question we asked was how the width of the box hill affects the quality of the numerical solution. A snap-shot from a simulation is shown in Fig. 10,
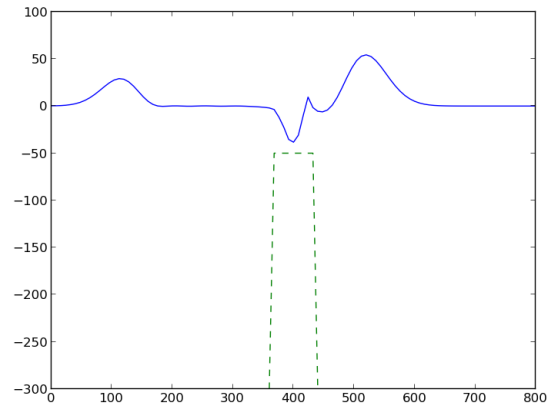
Figure 1: A snapshot of a one-dimensional simulation with a box-shaped hill at the bottom of the sea. The solution is clearly not smooth, and has probably numerical noise.
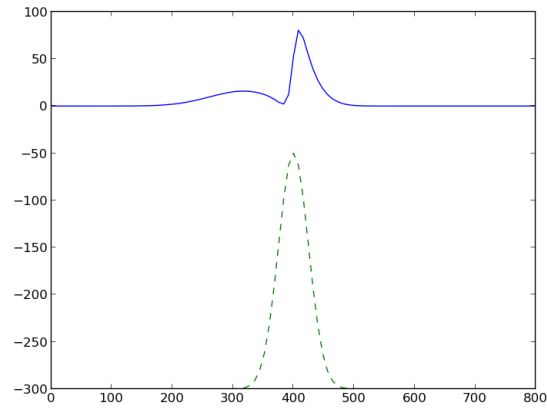

Figure 2: A picture from a one-dimensional simulation with a Gaussian-shaped hill at the seabed. This solution is smoohter than the result of the simulation with a box-sahped hill, but is partially quite sharp.
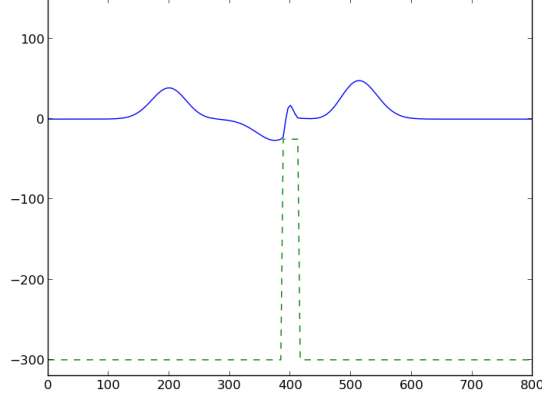
Figure 3: An example from a simulation with a narrow box hill. The resulting function is more spectacular than what was obtained with a wider box.

and the movie is stored in the directory `movie_1dwave_box_Ba275_Bs15_Nx200`. At least, the solution is more spectacular with a narrower box perturbation. Still, it is not possible to say whether this is due to numerical noise or an oscillating shape of the exact solution. Intuitively, it is plausible that a geometry with sharp forms gives rise to high-frequency components, which in turn may lead to sharp and/or oscillating solutions. Generally, we observed that there were very clear reflections of part of the wave at the discontinouity points of the q function. When using smoother hills, the reflections became more spread out.

The latter observation was studied closer using discontinuous and smooth step functions. The smooth step function was of the form

$$B(x, y) = B_0 + \frac{B_a}{1 + \exp\left(-(x - B_{mx})/B_s\right)}, \tag{28}$$

where B_0, B_a, B_{mx}, and B_s are parameters. These geometries might be used to simulate a tsunami approching a shore where the sea level decreases suddenly. The related movies are stored in the directories `movie_1dwave_box_shore` and `movie_1dwave_smooth_step`. We found that the reflected wave was sharper peaked in the case with a discontinuous step function, whereas the smooth step function gave a reflected wave more smeared out. However, both simulations had similar sharp oscillations behind the main wave. This oscillation may be a numerical artefact. One can also observe how the wave moves slower on the shallower water. This is natural, as the function $q(x, y)$ is proportional to both the depth of the sea, $B(x, y)$, and the squared of the wave velocity, c^2. From a physical point of view, the wave uses energy to keep the wave pulse higher, and therefore has less energy left for moving horisontally.
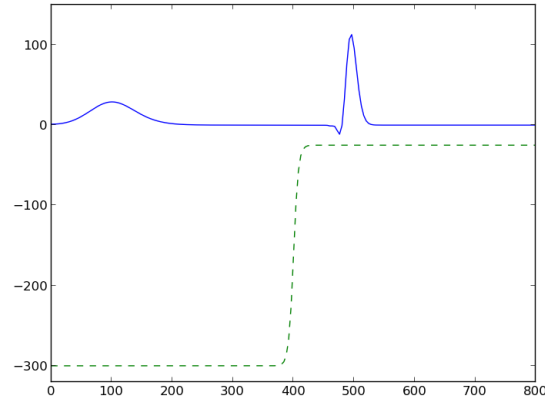
8

Figure 4: A smooth step function is used at the shore. The reflected wave pulse is more smeared out than in the case with a sharp step function. This result shows oscillations behind the main pulse, which may be numerical noise.
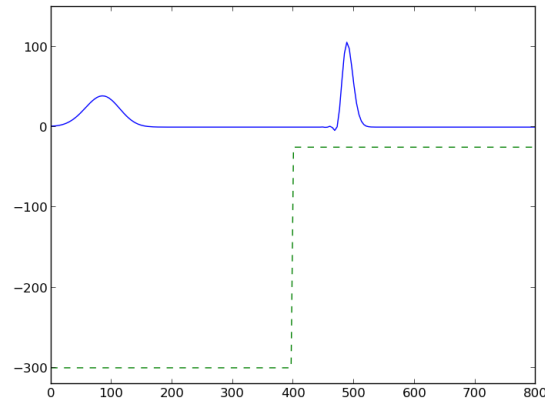

Figure 5: The shore is modelled using a sharp step function. In this case the reflected wave is sharp. As in the case with a smoother step function, here is also seen oscillations behind the main wave pulse.
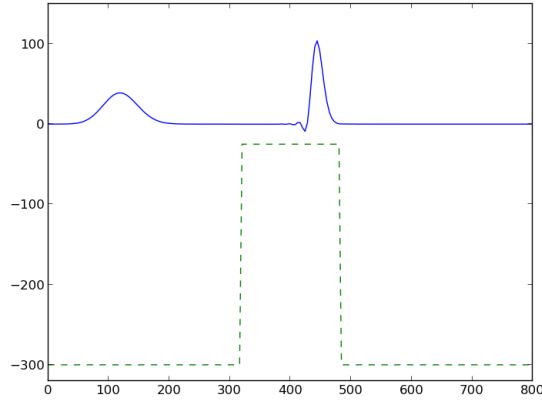
Figure 6: The last frame of the small box with no gap movie.

5.3 One-dimensional hill w/ gap simulations

In the other test we've run so far the hill has only been discontinous at the edge. What happens if we introduce a discontinous gap at the top of the hill? Letting b(x,y) be the usual shape of the hill, M_x be the x-coordinate of top of the hill, B_m be the height of the seabed and ϵ be the length of the slit we introduce the funcion:

$$b_s(x,y) = \begin{cases} b(x,y) & \text{if } (M_x - \epsilon) \leq x \leq (M_x + \epsilon) \\ B_m & \text{otherwise} \end{cases}$$

For the choice of b we have several good choices. For our simulation we chose two which seemed radically different: The continous gaussian bell shape and the discontinous box shape. They were ideal as we'd already studied their behaviour without a gap.

The difference between M_x and B_m were chosen large to make the discontinous border of the hill longer and hopefully make an eventual numerical instability more visible. ϵ is chosen to be small compared to the size of the hill. One might imagine a discontinuity at a single point might cause more trouble than one spanning several points, so $\epsilon = 0$ is also tested.
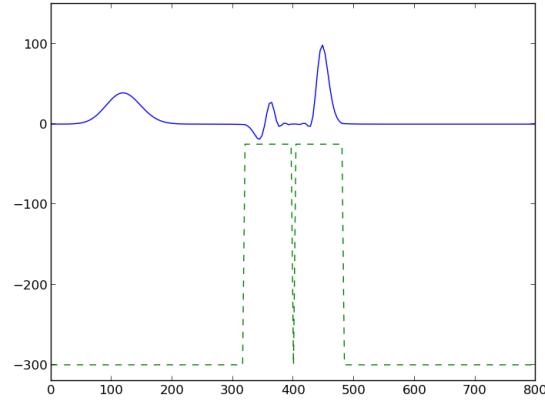
5.4 Plots of hills w/ gap

10

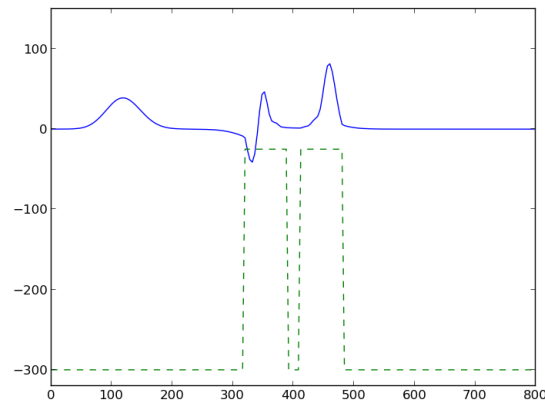Figure 7: The last frame of the box with 1 point gap movie.

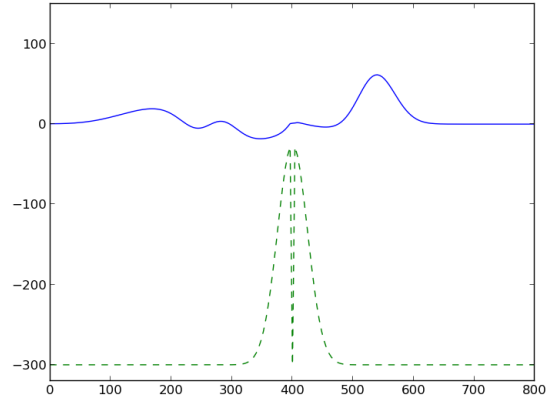Figure 8: The last frame of the box with 10 point gap slit movie.

11

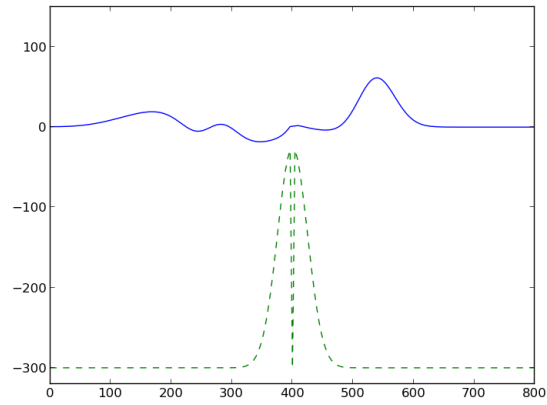Figure 9: The last frame of the gaussian hill with 1 point gap movie.

Figure 10: The last frame of the gaussian hill with 1 point gap movie.

6 Conclusions

6.1 One-dimensional hill w/ gap simulation conclusions

For the gaussian hill introducing a gap did not seem to cause much numerical instability. While the wave behaved differently than it did for the gapless hill, it stayed relativly smooth throughout the simulation and seemed to fit somewhat with the physical properties of such a wave. For the box hill the gap caused more problems. While the was at times rather steep and the wave propogated into the hill at one point.

One might then be tempted to conclude that having otherwise smooth hills mitigates the effect of a gap in the middle, but this is not necissarily true. The reflected wave from the gap did not in any of the tests seem to reflect back and interact with the main wave while it was in the gap, so the only difference the hill shape should have would be the shape of the wave hitting the gap. It does not seem unreasonable that a wave in the shape of the wave generated by passing over the box hill could also be generated using a smoother hill. If this is the case, would not a gap in this hill cause the same problems as we saw for the box? I find it more likely the steepnes of the wave is causing the instability in the box hill case, though this could in turn be connected to the steepness of the hill.

The one point gap simulations mirrored the ten point gap simulations and did not seem to cause any additional problems. If anything both simulations seemed more stable than the ten point counterparts. It is still worth noting the huge impact such a point has on the solution. If the gap is not mirrored in the physical case (say it is a measuring error) one can get huge differences between the simulated solution and the real behaviour of the phenomena.